




Article

First Principles Study and Experimental Investigation of Graphene-Molybdenum Disulphide Nanocomposites Based Passive Saturable Absorber

Siti Nabilah Mohd Halim ¹, Fauzan Ahmad ^{1,*}, Muhammad Quisar Lokman ¹, Husni Hani Jameela Sapongi ¹, Mohamad Fariz Mohamad Taib ², Wan Mohd Fazli Wan Nawawi ³, Hafizal Yahaya ¹, Mohd Azizi Abdul Rahman ¹, Suhaidi Shafie ⁴ and Sulaiman Wadi Harun ⁵

¹ Malaysia-Japan International Institute of Technology (MJIIT), Universiti Teknologi Malaysia, Jalan Sultan Yahya Petra, Kuala Lumpur 54100, Malaysia

² Faculty of Applied Sciences, Universiti Teknologi MARA, Shah Alam 40450, Malaysia

³ Department of Biotechnology Engineering, Kulliyah of Engineering, International Islamic University Malaysia, Kuala Lumpur 50728, Malaysia

⁴ Department of Electrical and Electronic Engineering, Faculty of Engineering, Universiti Putra Malaysia (UPM), Serdang 43400, Malaysia

⁵ Photonics Engineering Laboratory, Department of Electrical Engineering, Faculty of Engineering, University of Malaya, Kuala Lumpur 50603, Malaysia

* Correspondence: fauzan.kl@utm.my



Citation: Mohd Halim, S.N.; Ahmad, F.; Lokman, M.Q.; Sapongi, H.H.J.; Mohamad Taib, M.F.; Wan Nawawi, W.M.F.; Yahaya, H.; Abdul Rahman, M.A.; Shafie, S.; Harun, S.W. First Principles Study and Experimental Investigation of Graphene-Molybdenum Disulphide Nanocomposites Based Passive Saturable Absorber. *Photonics* **2022**, *9*, 704. <https://doi.org/10.3390/photonics9100704>

Received: 25 August 2022

Accepted: 21 September 2022

Published: 28 September 2022

Publisher's Note: MDPI stays neutral with regard to jurisdictional claims in published maps and institutional affiliations.



Copyright: © 2022 by the authors. Licensee MDPI, Basel, Switzerland. This article is an open access article distributed under the terms and conditions of the Creative Commons Attribution (CC BY) license (<https://creativecommons.org/licenses/by/4.0/>).

Abstract: Research on hybrid graphene with other two-dimensional materials has gained considerable attention owing to their potential applications beyond single components. Through our first principles analysis via density functional theory, graphene-molybdenum disulphide (MoS₂) demonstrated a band gap opening by 2 meV, from gapless graphene when MoS₂ layer is introduced into the structure. The simulated graphene-MoS₂ has a direct band gap situated at K point of Brillouin zone with preserved Dirac properties of graphene. The experimental studies on graphene-MoS₂ also have been performed by preparing graphene-MoS₂-chitin nanocomposite through facile liquid-phase exfoliation method. Apart from energy gap using Tauc relation, the physical morphology and nonlinear properties of the material were systematically characterized. Graphene-MoS₂-chitin exhibits a modulation depth of 10.5%, which is lower than individual graphene but higher than individual MoS₂. Further investigation on the material's performance was done by integrating the fabricated film into Erbium-doped fiber laser. Stable nanosecond pulse laser operation was realized with graphene-MoS₂-chitin hybrid saturable absorber. The pulse width was measured to be 156.4 ns with repetition rate of 1.89 MHz, corresponding to a peak power of 56.13 mW and pulse energy of 8.78 nJ.

Keywords: density functional theory; graphene-MoS₂; saturable absorber; nanosecond pulse; erbium-doped fibre laser

1. Introduction

The discovery of two-dimensional (2D) graphene offers plenty of opportunities for the next generation of optoelectronic technologies due to its unique and distinctive properties. The gapless nature of graphene has led to wavelength-independent absorption, which makes it suitable for broadband spectrum applications [1]. Graphene also possesses high carrier mobility and nonlinear optical response to assist in saturable absorption with ultrafast recovery time. However, the absence of bandgap resulted in low light absorption intensity of 2.3% per one atomic layer and a large on-off ratio for graphene-based electronic devices, which can be seen as a limitation in certain applications [2]. Due to that, a significant number of other 2D materials similar to graphene properties have been actively pursued. To date, 2D materials such as transition metal dichalcogenides (TMDCs),

phosphorene, topological insulators (TI), and MXenes have shown remarkable saturable absorption properties with tunable band structures, quantum confinement, high carrier mobility and light absorption coefficient, and layer-dependent optical properties [1–3]. Molybdenum disulphide (MoS_2) is an exciting counterpart of the TMDC group, which has been extensively explored experimentally and theoretically [4] with layer-dependent bandgap properties of 1.1 to 2.0 eV. Owing to this band structure behaviour, they can be used in photonic and optoelectronic devices.

In order to broaden the scope of 2D materials for further application, significant research efforts have been devoted to the hybrid nanocomposite and formation of van der Waals (vdW) interactions made from layer-by-layer 2D materials. This makes ultrathin device development possible, possessing interesting properties far beyond their single component [5]. The structural, electronic, and transport properties has been studied theoretically [6–9]. The simulation work from Hu and Yang [9] proved that the 2D hybrid materials always possess a stronger optical absorption and wider absorption range compared to the individual monolayers as the carriers' transition can quickly occur within the interfaces of different layers. In addition, the hybridization of graphene and 2D material allows opening of graphene bandgap, which consequently leads to extensive exploration in the area of field effect transistor [6], photovoltaic [9], and laser devices [10–13]. In laser applications, the hybrid material possessed enhanced interlayer coupling, carrier dynamics, and nonlinear optical properties that is an essential quality to be based material for saturable absorber (SA).

The conventional mechanical exfoliation from scotch tape approach is the initial successful method to prepare graphene in its 2D form [14]. The method offers a 2D material characteristic with large grain size. However, the inability of producing graphene flake size lower than ten microns for large scale production is the main draw-back of this method, thus, making it unsuitable for practical application. Thereafter, chemical vapor deposition (CVD) technique successfully overcame the drawback with a promising quality yield at a larger production scale [15]. Numerous reported works with CVD-assisted to allow 2D materials fabrication with specific layered configuration. Unfortunately, the limitations exist from the high-cost instrumentation, the required high temperature with vacuum environment involved, lack of scalability and repeatability as well as impurities drawn inside the large surface area of material's layer. On the other hand, liquid-phase exfoliation (LPE) has become one of the eminent methods of choice among researchers for 2D materials fabrication [1]. The LPE method allows exfoliation of bulk crystal of the starting material to form nanosheet with reduced dimensionality. The formation of 2D layer consequently offers large surface area embedded in the host polymer for better absorption properties. Furthermore, the in-corporation of polymer helps the process of reducing crystallinity to increase the ionic conductivity of proposed samples. When the size of particles becomes smaller (much smaller than the visible light wavelength), the particles contribute less to scattering of light [16].

Graphene/ MoS_2 nanocomposite SA prepared from hydrothermal method [17], chemical vapor deposition [10], and monolayer intercalation method [11] have been successfully employed in Erbium doped fiber laser (EDFL), Ytterbium solid-state bulk laser, and Nd:GdVO₄ crystal laser, respectively, to demonstrate pulse laser generation. Particularly for EDFL, both mode-locking and Q-switching was realized by Jiang et al. [17]. A maximum repetition rate of 3.47 MHz and 21.9 kHz and pulse width of 2.2 ps and 9.31 μs , respectively, was achieved by drop casted the synthesized MoS_2 /graphene solution directly onto the fiber ferrule. Among the techniques for integration of SA into the cavity, direct deposition has been chosen in most graphene/ MoS_2 studies [10,11,17]. According to [18], the composite form of SA with polymer allows for better handling and mechanical tolerance as well as overcome the limitation on the reproducibility of the direct deposited SA [19]. Due to that, the preparation of SA embedded in a polymer such as polyvinyl alcohol (PVA) and polyethylene oxide (PEO) often favorable. Recently, bio-host polymer made from natural resources is used in fiber laser application. Chitin, is used as a non-toxic alternative to the

common synthetic polymer and proved has comparable properties. Zuikafly et al. [20] is the first reported work for chitin as a host polymer in SA fabrication and successfully demonstrated the Q-switching operation with highest repetition rate of 111.77 kHz and lowest pulse width of 1.328 μ s.

Herein, the proposed SAs were prepared by liquid-phase exfoliation embedded with a bio-host chitin. With combined techniques from LPE method and composite polymer form, the developed graphene-MoS₂-chitin from this work offers simplicity, and a reliable approach to demonstrate pulse laser generation, particularly in Q-switched regime. Simultaneously, theoretical simulation through density functional theory (DFT) calculation is employed to investigate the properties of materials at the atomic level.

2. Theoretical Method and Analysis

First principles calculation was performed in the framework of DFT as implemented in the Cambridge Serial Total Energy Package (CASTEP) simulation software. Suitable choice of functional parameters is important for geometrical optimization and properties calculations. From the convergence test results, the Perdew-Burke Ernzerhof (PBE) exchange-correlation functional with general gradient approximation (GGA) functional was taken for electron exchange and correlation. Ultra-soft pseudopotential was employed for the calculations of electronic interaction with 12 valence electrons of Mo ($4p^6, 5s^1, 4d^5$), six valence electrons of S ($3s^2, 3p^4$), and four valence electrons of C ($2s^2, 2p^2$). The plane-wave functions basis set with cut-off energy limited at 380 eV as increasing the value to 400 eV did not give any significant change in the total energy of the system. All atomic positions in the supercell have been relaxed according to the cell optimization criterion, such as displacement of 5.0×10^{-4} Å, force of 0.01 eV/Å, and self-consistency field (SCF) tolerance of 5.0×10^{-6} eV/atom. The plane-wave Monkhorst-Pack k-point was sampled by $4 \times 4 \times 1$ for the relaxation and total energy calculations. The optimized model structure of graphene-MoS₂ was constructed using a 4×4 graphene and 3×3 MoS₂ supercell with a vacuum slab of 15 Å to have a smaller lattice mismatch and prevent periodic interaction. Some selected criteria and values were adopted from available literature [7,21,22] as guided references. A small supercell with adequate atomic number was employed as larger supercell consumes more time and computational cost for DFT calculation to be done. The simple model of atomic structure for graphene, MoS₂, and graphene-MoS₂ are shown in Figure 1a, 1b, and 1c, respectively. Graphene consists of hexagonal bonded carbon atoms, while MoS₂ consists of S-Mo-S layer with Molybdenum (Mo) atoms arranged in trigonal prismatic coordination between the two Sulphur (S) layers. Meanwhile, the optimized atomic configuration of graphene-MoS₂ was confirmed with previous study by [21,22]. The adjacent layers of the heterostructure are held together by vdW force at the selected active site.

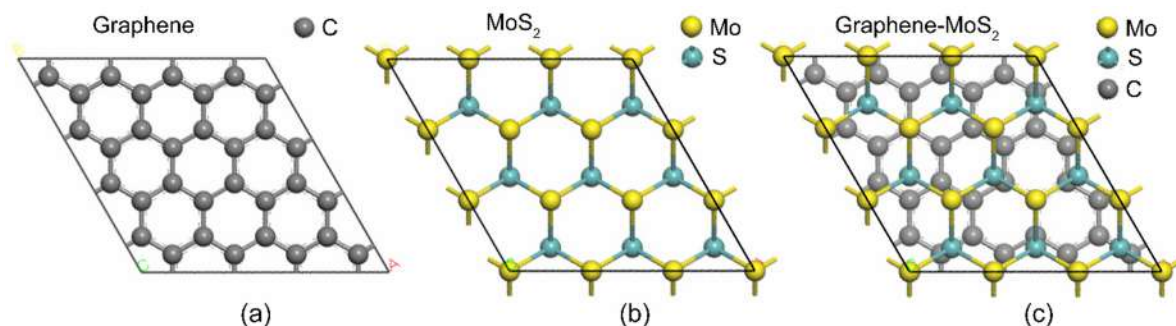


Figure 1. Atomic structure of (a) graphene, (b) MoS₂, and (c) graphene-MoS₂.

In order to explore the electronic structure properties of graphene-MoS₂, DFT calculations on typical electronic band structures have been performed and illustrated in Figure 2. The band structures were plotted along the high symmetry point in Brillouin zone (BZ) to observe the energy band gap (E_g). The E_g can be determined by the opening gap be-

tween valence band maximum (VBM) and conduction band minimum (CBM) of occupied state presented in band structure with Fermi level equal to zero. As shown in Figure 2a, graphene exhibits a gapless nature with formation of Dirac cone at the Fermi level. The zero-energy band gap of graphene was in excellent agreement with other reported work in literature [7,21,22]. Theoretically, due to zero gap, electrons and holes inside atomic structure can freely move, thus resulting in fast carrier dynamics and broad wavelength coverage as it possesses wavelength-independent absorption [7].

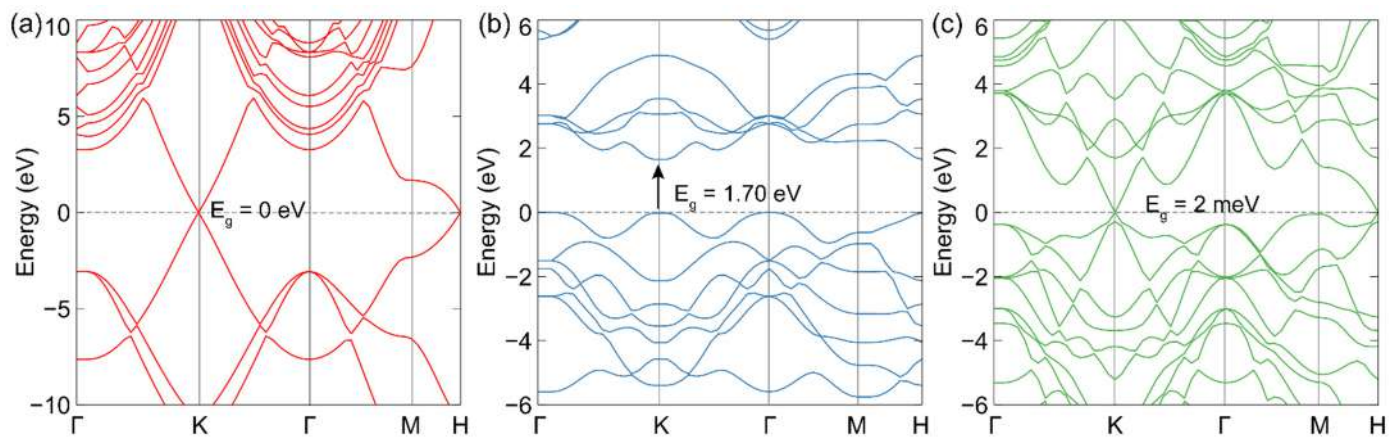


Figure 2. Theoretical band structure of simulated (a) graphene, (b) MoS₂, and (c) graphene-MoS₂.

Meanwhile pure monolayer MoS₂ shows a direct band gap with value of 1.70 eV which is consistent with other theoretical report ~1.8 eV [23], ~1.73 eV [24] and ~1.7 eV [25]. Upon hybridization of graphene and MoS₂, the VBM and CBM are situated along the high symmetry K point of BZ, confirming the direct type of band gap with a small magnitude equal to 2 meV. The calculated band gap value has been validated with previous theoretical study, which is 8.3 meV [21], 3.6 meV [22], 0.4–1.1 meV [23], 3.49 [24] and 27 meV [8]. In principle, a direct band gap materials are optically active semiconductor, thus making them preferable in most photonic devices, while the indirect gap compounds show relatively less optical excitation and emission as the transition is associated with phonon energy [25]. The Dirac properties of graphene is also preserved near the Fermi level even with the modulation in band gap energy, as shown in Figure 2c. From the result, the band gap tuning can be attributed to the increase in crystallinity due to the variation of the interlayer coupling strength, resulting in higher atoms mobility with MoS₂ acting as the transition metal material donating the holes to the graphene [23,26]. The existence of energy gap in band structure can entail optical absorption edge which corresponds to the intra- and inter-band electron transitions from occupied to unoccupied states. The charge transfer and quantum confinement between two hybrid materials thereby making them optically active.

In addition, the investigation on the origin of band structure for graphene-MoS₂ is required to identify the contribution of electronic states from different orbital of the constituent atoms. Therefore, the total and partial density of states (DOS) of graphene-MoS₂ is computed and illustrated in Figure 3. The green box highlighted in the Figure 3 is where Fermi level and band gap is located inside atomic structure. It is demonstrated that the prevailing contribution to the total DOS at the VBM is primarily from the upshifted of Mo-*d* and S-*p* orbital of MoS₂. The *d* and *p* orbital are the lowest electronic state in the atomic arrangement of MoS₂, which signifies the active optical elements and is mainly responsible for the electronic transition inside the band gap [22]. Meanwhile, the DOS for graphene preserved its Dirac property near the Fermi level. Therefore, the band gap of graphene hybrid can be tuned through the variation in MoS₂ concentration to determine an optimized ratio in hybridization materials [17,22].

Optical characterization can be modelled by the complex dielectric function of the material system derived from the Kramers-Kronig relation, $\epsilon(\omega) = \epsilon_{\text{real}} + \epsilon_{\text{imaginary}}$ with

function of photon energy (ω) [25]. The real part of dielectric constant is complex permittivity associated with polarization of light caused by the applied electric field, while the imaginary part is related to the optical absorption of photon (loss or gain) of the material [13,14]. The equation can be expanded to other optical constants such as refractive index, absorption coefficient, reflectivity, and energy loss spectrum. The simulated real and imaginary parts of dielectric function of graphene, MoS₂, and graphene-MoS₂ are shown in Figure 4a,b. The dielectric functions of graphene and MoS₂ material have highly anisotropic properties at low energy regions and become isotropic towards high energy region, which is similar to other studies [24,27]. Since optical constant is wavelength dependent, low energy zone ranging from infrared, visible to ultraviolet region is more preferable to be explored, particularly at telecommunication region of 1550 nm or 0.8 eV for photonics application.

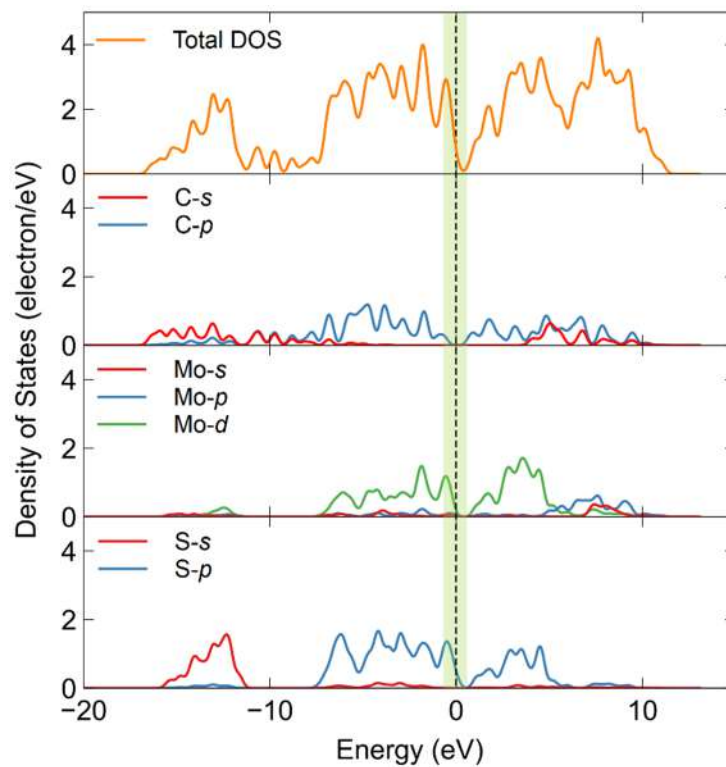


Figure 3. Total and partial of states of simulated graphene-MoS₂.

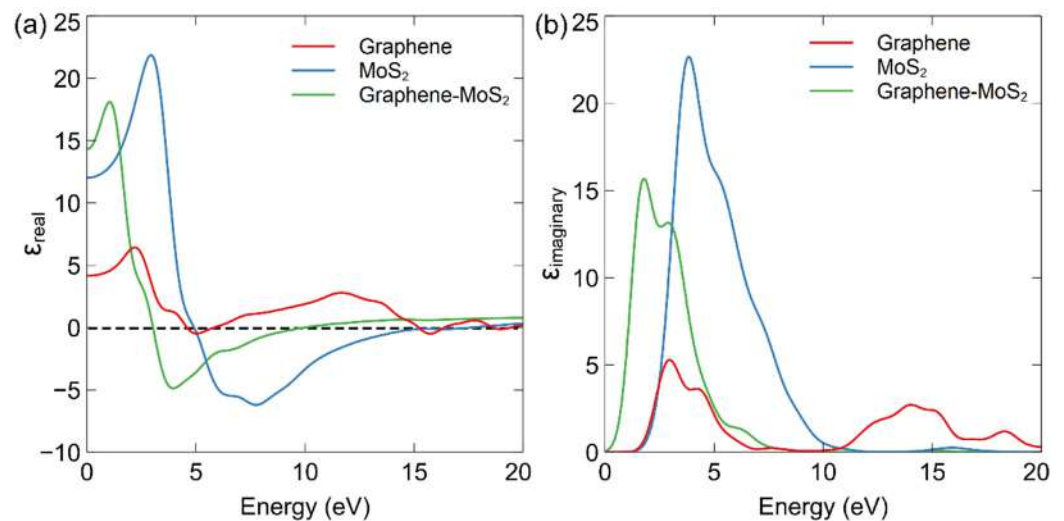


Figure 4. Theoretical real and imaginary part of dielectric function of simulated graphene, MoS₂, and graphene-MoS₂ (a) real and (b) imaginary.

The value of static dielectric constant of pure graphene at 0.8 eV was 4.2, with prominent peak at 2.0 eV. The simulated result showed an agreement with previous study by Qiu et al. [24] that obtained the same trend with value of dielectric constant about 4.5 at low energy region and significant peak at 2.5 eV. For imaginary part, a significant peak at 3 eV was observed, which originates from the inter-band transitions according to the interpretation by previous reported work [27]. The same trend can be seen for dielectric function of MoS₂ structure, except it has a high dielectric constant value at 0.8 eV, which is about 12.4 with prominent peak at 4.0 eV. The value is consistent with previous reported work by Hieu et al. [25], which records dielectric value of 15.01 and significant peak at 3.5 eV. Meanwhile, as graphene and MoS₂ were stacked together, the dielectric constant was modulated to a value of 14.4 and significant peak at 1.6 eV. The transition of real part from positive to negative intersect at 3.1 eV indicate that graphene-MoS₂ should resonate at energy higher than that 3.1 eV [26]. The imaginary part shows an increase of spectrum compare to the individual graphene plots, which is reflected to the rise of electronic interaction inside the material [24]. This imaginary part is directly providing the absorption spectra analysis, which has been further illustrated in Figure 5.

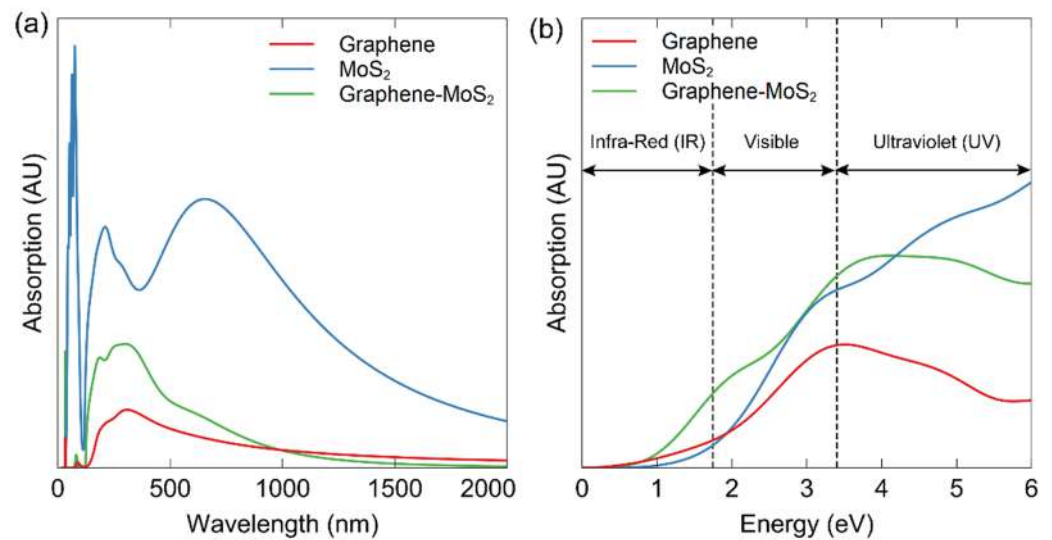


Figure 5. Theoretical absorption spectrum of graphene, MoS₂, and graphene-MoS₂ as a function of (a) wavelength and (b) energy.

Figure 5a shows the simulated absorption spectrum with respect to wavelength and photon energy in the inset. The absorption peak at 225 nm from graphene corresponds to the typical π - π^* transition of aromatic C-C bonds in the graphene network [28]. Similar trend can be observed when MoS₂ is incorporated into graphene network with larger absorption peak. The increase in absorption peak indicates the absorption properties of graphene was preserved but exhibit a greater conjugated π bonds at the increased material concentration as described by Beer-Lambert law relation [29]. For MoS₂, the absorption spectrum consists of characteristic peaks at around 400–450 nm ascribed from the excitonic transitions within high-density of states in Brillouin zone [30].

In parallel, absorption spectrum with respect to energy was shown in Figure 5b to confirm the accessible wavelength region for the three models' structures. The absorption intensity of graphene was recorded as the lowest with broadest spectrum covering from infrared to ultraviolet region. This is in agreement with the well-known broadband wavelength range from the optical characteristic of graphene [1–3]. The results also agree with the absorption spectrum at low energy region below 2 eV as reported by Qiu et al. [22]. Meanwhile, optical absorption coefficient can be obtained from the absorption edge at the intersection of reverse tangent and x-axis of lower energy region. It corresponds to the electronic transition inside the materials with binding energy and describes optical gap of material. The simulated optical gap of graphene, MoS₂, and graphene-MoS₂ is

0.45 eV, 1.62 eV, and 0.69 eV, respectively. The values were comparable with the data from previous work [24], which recorded optical gap of 0.75 eV for graphene, 1.63 eV for MoS₂, and around 0.41 eV to 1.40 eV for graphene-MoS₂. The optical gap of graphene-MoS₂ was averagely low, allowing the photoelectron to be excited with less energy [24,28]. Besides that, the calculated absorption spectrum proved that hybrid of graphene-MoS₂ possesses a broadband wavelength range from infrared, visible to ultraviolet regions with significant increase in absorption intensity compare to individual graphene, leading to a widespread application.

3. Material Fabrication and Characterization

Three samples were fabricated, which are graphene-MoS₂, graphene, and MoS₂ with chitin as a host polymer to form SA film and the process is as follows. Graphene filament was employed as the starting material for the preparation of graphene suspension. Initially, graphene-poly(lactic acid) (PLA) filament (Conductive Graphene Composites, Black Magic 3D) with a diameter of 0.4 mm was extruded through a 3D printer nozzle to reduce its diameter to a desired 400 µm for easier processing. The composition of the filament consists of graphene platelets (30–40%), poly(lactic acid) (25–35%), Tris(nonyl phenyl)phosphite (5–10%), and carbon fibers (5–10%) which can be retrieved from blackmagic3d.com [31] website. The extruded filament was weighed at approximately 25 mg and added into 10 mL of tetrahydrofuran (THF), producing graphene slurry in THF solution. The graphene-PLA-THF suspension then underwent ultrasonication in ultrasonic bath for 10 min. For MoS₂ suspension, 5 mg of MoS₂ powder (Sigma Aldrich, St. Louis, MO, USA, particles diameter of ~100 nm, purity 99%) was dissolved homogeneously in 5 mL of THF solution under magnetic stirring at ambient temperature and 1000 rpm for about two hours.

Extraction process of chitin biopolymer used in this research was based on Wan Nawawi et al. [32]. Chitin nanofiber was extracted from frozen oyster mushrooms (*Pleurotus ostreatus*) using mild alkaline treatment to preserve the amorphous glucans within the matrix. The frozen mushrooms were thawed and blended for 5 min with a high-speed mixer (Vita Mixer Innofood, SX766) to break the cell wall. After that, water-soluble components were removed by hot water treatment under stirring conditions (85 °C, one hour). The suspension was filtered with a cotton filter cloth before the wet cake was being left to soak in 1 M sodium hydroxide for 3 h at 65 °C. The suspension was then neutralized using the filtration process and the neutralized wet cake was diluted with distilled water (0.4% w/v). For homogenous dispersion, the chitin dilution was post-blended for 5 min and kept stable at 4 °C until further use.

Solution-process of graphene-MoS₂ hybrid was done by mixing an equal amount of 1.25 mL graphene and MoS₂ solution into 2.5 mL of chitin biopolymer. Altogether, the ratio of graphene-MoS₂ to chitin is 1:1 ratio summing up to 5 mL in volume. The 5 mL value was chosen to ensure the solution could be filled into the circular petri dish with 3.5 cm diameter and 1.0 cm height producing film with thickness of around 30 µm to 50 µm. Then, the mixed solution was placed in ultrasonic bath for about three hours to ensure a well-homogenized dispersion. Ample time of sonication process allowed exfoliation of bulk crystals into nanosheets as the van der Waals interaction weakened due to production of microjets and shockwaves from collapsing cavitation bubble [33]. The obtained dispersion mixture was then poured into a petri dish and let dry at ambient temperature for about 48 h before they were ready to be peeled off as a free-standing film SA. Meanwhile, individual graphene-chitin SA was fabricated by mixing homogeneous graphene-PLA-THF with chitin in 1:1 ratio, sonicated in ultrasonic bath for two hours and poured into petri dish before letting dry for two days. At the same time, by using the same process, the homogeneous MoS₂-THF suspension was mixed with chitin in 1:1 ratio to produce MoS₂-chitin based SA.

The SA films undergo structural characteristic evaluation before further demonstration of their effectiveness in pulsed fiber laser operation. The morphology of extracted fungal chitin was observed using field emission electron microscope (FESEM) (Hitachi, Tokyo, Japan, SU 8030) at 1 kV accelerating voltage, while graphene-chitin, MoS₂-chitin,

and graphene-MoS₂-chitin were observed from model JSM-7800F (JEOL, Tokyo, Japan). Figure 6a highlighted the fibrous structure of chitin with blurry image contributed by the amorphous structure of glucans that bind a dense network of fibers. As chitin becomes polymer for all developed samples, the fibrous network with tube or string-like formation and large surface area of flaky image dominates the whole composition surface as can be observed in Figure 6b–d. This is denoted to the material embedded uniformly into the chitin bio-host polymer. In addition, all obtained FESEM image denotes a uniform distribution with no bubbles, hole, or crack which is vital for material's performance in terms of ensuring lower amplitude fluctuations during pulse laser generation [1]. Figure 6e,f shows the thickness profile of graphene-MoS₂-chitin which was measured using 3D laser scanning microscope (Olympus, Tokyo, Japan, OLS 4100). The thickness was measured by the difference in height of the graphene-MoS₂-chitin and microscope stage. The measured thickness is around 33.82 μm which is consistent with other reported film thickness of around 30–50 μm [34]. In addition, the thickness of the graphene-chitin and MoS₂-chitin should be similar with the graphene-MoS₂-chitin due to the thickness of the SA is determined by the amount of sample solution before dry casting process.

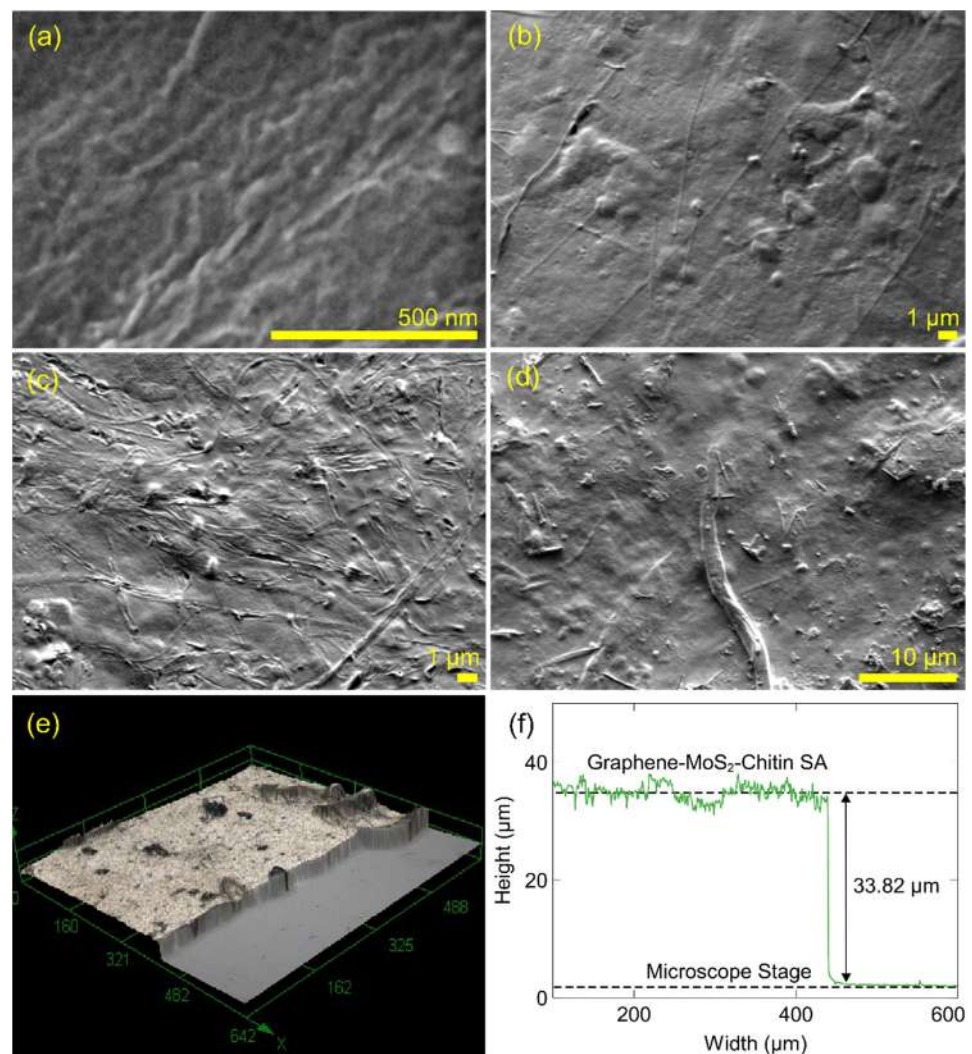


Figure 6. FESEM image of (a) chitin, (b) graphene-chitin, (c) MoS₂-chitin, (d) graphene-MoS₂-chitin, (e) 3D image profile and (f) thickness measurement from laser microscope.

Figure 7 reveals the Raman spectrum of the fabricated film which will confirm the materials' existence through key spectrum peaks identifiers resulted from the vibrational modes of material. In pure graphene Raman spectrum, due to the vibration of sp²-bonded

carbon atoms, the two prominent characteristic peaks of D-band and G-band of graphene layer at 1390 cm^{-1} and 1584 cm^{-1} are clearly displayed in the figure. The single layer graphene can be analysed from the peak intensity ratio of the 2D and G is equal to 2 or expressed by $I_{2D}/I_G = 2$ [35]. This expression is true if the graphene has sharp symmetric peak, which confirms the high quality and defect-free graphene sample. Since the obtained peak from the Raman spectrum is not sharp and symmetric, this indicates that the developed graphene is not defect-free and has relatively high number of layers produced. The fact that LPE method is employed, it is worth mentioning that structural defect cannot be avoided. Nevertheless, we had successfully confirmed the graphene existence in the sample through the Raman spectrum. Meanwhile, Raman peaks at E_{2g} and A_{1g} which are the characteristic peaks of the 2H-phase MoS_2 are confirmed at 376.59 cm^{-1} and 395.71 cm^{-1} respectively. For graphene- MoS_2 nanocomposite, the corresponding two significant peaks at 1357.03 cm^{-1} and 1574.58 cm^{-1} are in agreement with previous reported study [36]. As MoS_2 is introduced in graphene matrices, the G-band of graphene is down-shifted to 1574.58 cm^{-1} as a result of the softening of the atomic bond with addition of doping which also reveals the evidence of interlayer coupling inside the nanocomposite [36].

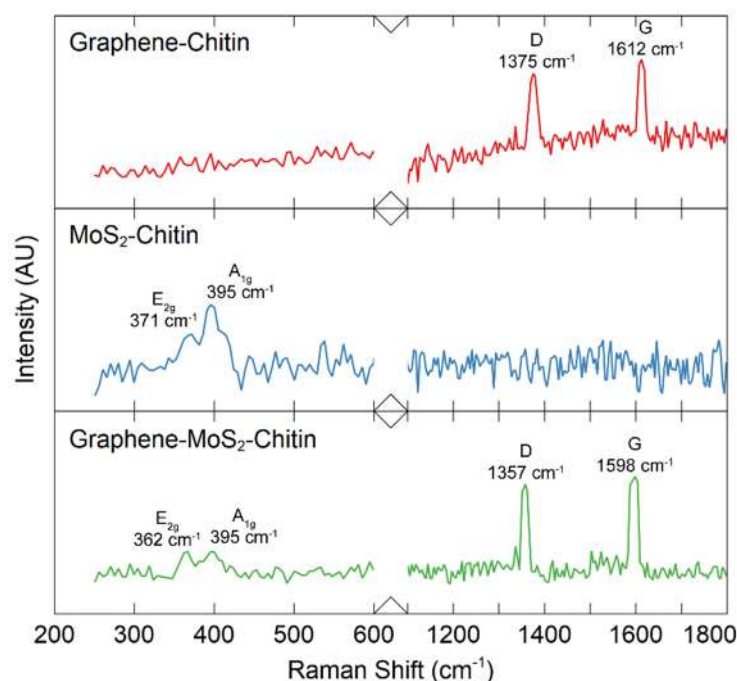


Figure 7. Raman spectrum of the fabricated graphene-chitin, MoS_2 -chitin, and graphene- MoS_2 -Chitin SA films.

Figure 8a shows the ultraviolet-visible-near infrared (UV-Vis-NIR) (Perkin-Elmer, Waltham, MA, USA, Lambda 750) transmission spectrum of graphene- MoS_2 , graphene and MoS_2 film to investigate the optical absorption and transmission response of the prepared materials. The transmission of 11.54% was recorded at a wavelength of 1550 nm for graphene- MoS_2 film which is lower than that of graphene (~33%) but higher than MoS_2 (~3%). The obtained value depicts that the incident light passing through the graphene- MoS_2 -chitin SA was reduced due to heightened absorption ability has been achieved. From the UV-Vis-NIR spectrum, the optical bandgap can be obtained by using Tauc plot method in which $(\alpha hv)^n$ was plotted as a function of photon energy (hv) where α is the linear absorption coefficient, hv is the incident photon energy and n can be $\frac{1}{2}$ or 2 for a direct and indirect allowed transition, respectively [37]. As shown in the Figure 8b–d, the linear fitting interception at x -axis and by fitting the suitable values of n in the Tauc relation gives the bandgap value. Based on the linear intercept, the value of band gap is comparable with those theoretical value obtained from the band structure in Figure 2. From the n

value, both Graphene-MoS₂ and graphene has direct bandgap of 0.628 eV and 0.259 eV respectively. Meanwhile, MoS₂ exhibit indirect band gap of 1.806 eV. It is expected that experimental value for graphene, MoS₂ and graphene-MoS₂ are slightly different from theoretical simulation mainly arises from the additional composition of the host polymer material such as chitin and the inevitably impurities throughout the fabrication process. Nevertheless, the result of Tauc relation is in agreement with the theoretical band structure in determining direct and indirect energy gap.

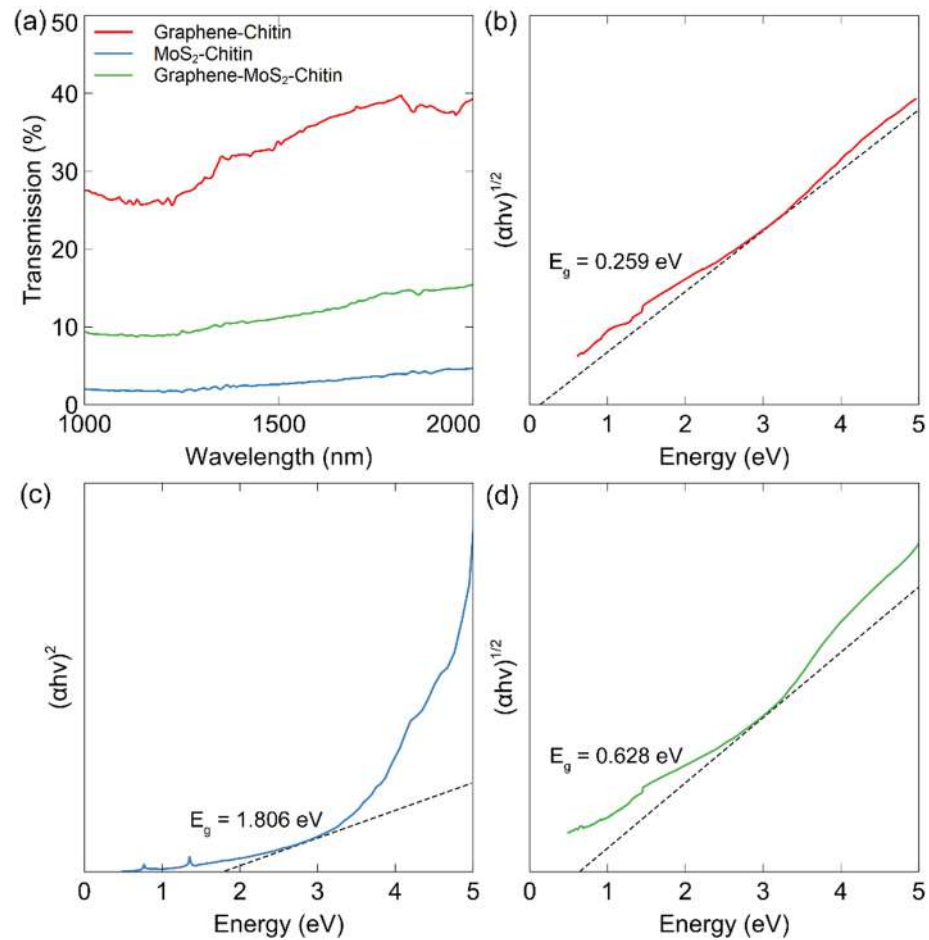


Figure 8. UV-Vis-NIR spectrum of graphene-MoS₂-chitin film; (a) transmission spectrum and Tauc plot of (b) graphene-chitin, (c) MoS₂-chitin, and (d) graphene-MoS₂-chitin.

The nonlinear absorption properties of the graphene-MoS₂ nanocomposite SA were investigated by a balanced twin detector method. In the measurement, the nanosecond pulse fiber laser with repetition rate of 1.89 MHz and pulse width of 191.6 ns was used as a light source. Figure 9 shows the experimental data and curves fitted by the following equation;

$$A(I) = \alpha_0 \cdot \exp\left(\frac{-I}{I_{sat}}\right) + \alpha_{ns} \tag{1}$$

where A , I , α_0 , I_{sat} , and α_{ns} is absorption, input intensity, saturable absorption (modulation depth), saturation intensity, and non-saturable absorbance coefficient respectively [38]. As shown in Figure 9, the highest modulation depth is shown by individual graphene at 19.0%, higher compared to previous graphene-based SA [39]. Meanwhile, graphene-MoS₂ SA has modulation depth of 10.5% with saturation absorption intensity of 2.40 kW/cm². The lowest modulation depth at around 6.06% is achieved by individual MoS₂ with saturation intensity of 2.40 kW/cm².

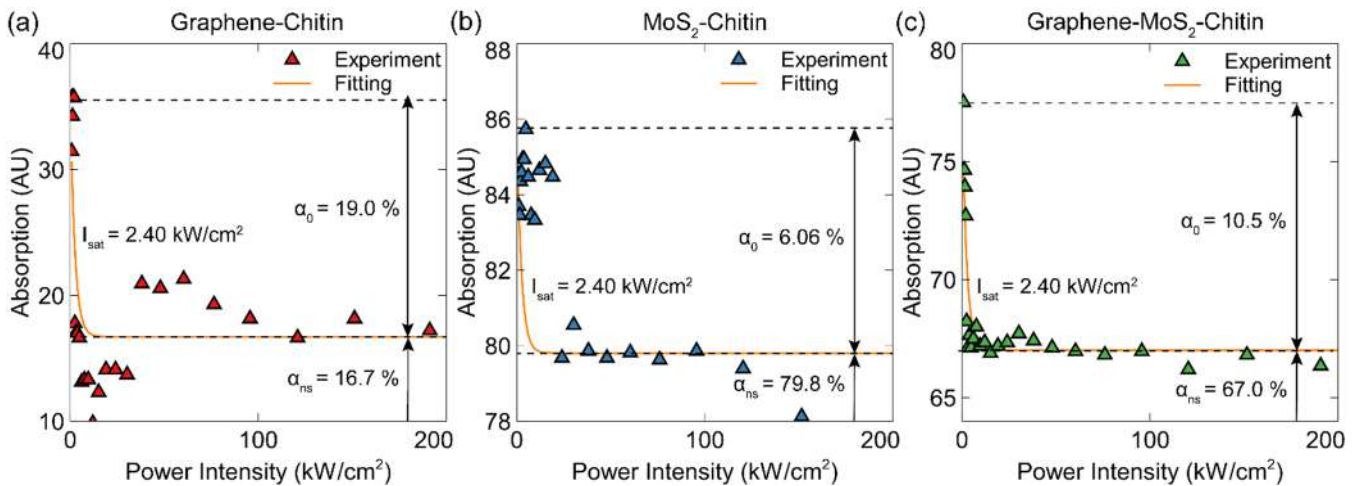


Figure 9. Non-linear absorption of (a) graphene-chitin, (b) MoS₂-chitin and (c) graphene-MoS₂-chitin.

4. Fiber Laser Setup and Nanosecond Pulse Performance

The fabricated SA film was integrated into an EDFL ring cavity by sandwiching it between two ferrules, as shown in Figure 10. The ring cavity consists of additional 100 m long standard single mode fiber (SMF) to tailor the dispersion characteristic and nonlinearity of the cavity, thus allowing a nanosecond pulse generation with the extension of the cavity length. The EDFL cavity works in anomalous dispersion with net total dispersion at around ~ 2.25 ps²/km. The output was tapped out by a 90/10 optical coupler, where 90% of the light is kept oscillating in the cavity, and the remaining 10% is used for output measurement to simultaneously observe the pulse train, signal-to-noise ratio, and optical spectrum through a 10 dB coupler. The laser outputs were obtained through an optical spectrum analyzer (Ando, Kanagawa, Japan, AQ-6370C) for optical spectrum trace and optical power meter (OPM, Thorlab, Newton, NJ, USA, PM100D) for output power measurement. A 5 GHz photodetector (Thorlab, DET08C) was connected to 500-MHz digital oscilloscope (GW Instek, New Taipei City, Taiwan, GDS3352) for pulse train and a 7.8 GHz Radio Frequency (RF) spectrum analyzer (Anritsu, Kanagawa, Japan, MS2683A) for signal-to-noise ratio (SNR) measurement. The overall length of this laser cavity was approximately 110 m.

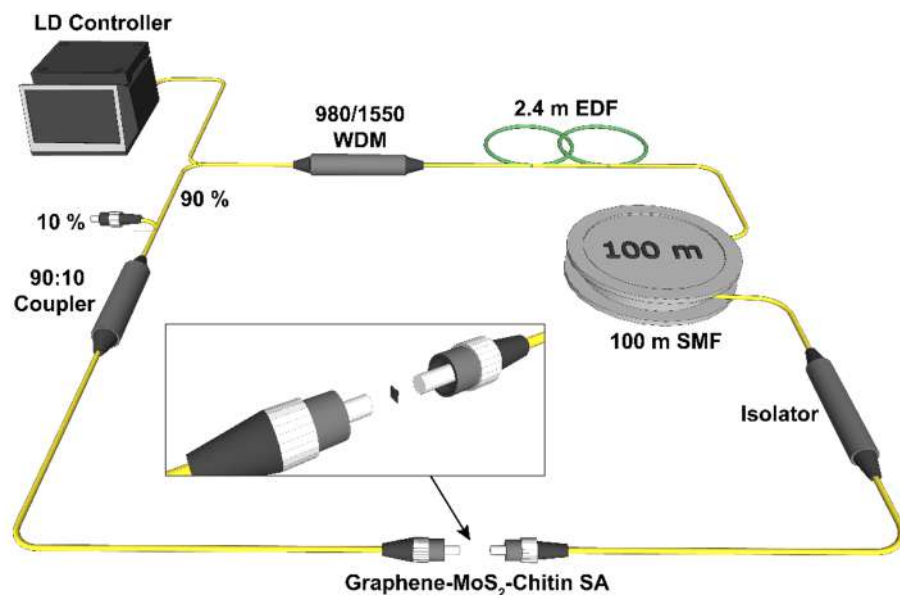


Figure 10. Schematic diagram of fiber laser configuration.

The performance of the pulsed laser generation was investigated by varying the 980 nm input pump power. Except for MoS₂-chitin, the developed SAs are able to realize nanosecond pulsed laser. Therefore, presented here are the nanosecond pulsed laser performance for graphene-chitin and graphene-MoS₂-chitin and Q-switched pulsed laser for MoS₂-chitin. Figure 11 shows the OSA trace for the developed SAs compared to the continuous wave (CW) spectrum. The CW wavelength was recorded at 1564.70 nm as depicted in Figure 11a. When the SAs were inserted in the cavity, the wavelength showed some shift as can be seen in Figure 11b–d for graphene-chitin, MoS₂-chitin, and graphene-MoS₂-chitin, respectively. At maximum pump power of 75.91 mW, the graphene-chitin SA exhibited an almost similar wavelength (~1564 nm) with graphene composite fabricated via electrochemical exfoliation proposed by Ismail et al. [39]. The operating wavelength of 1561.84 nm for graphene-chitin SA showed a slight shift from the CW with spectrum broadening of 0.48 nm as shown in Figure 11b.

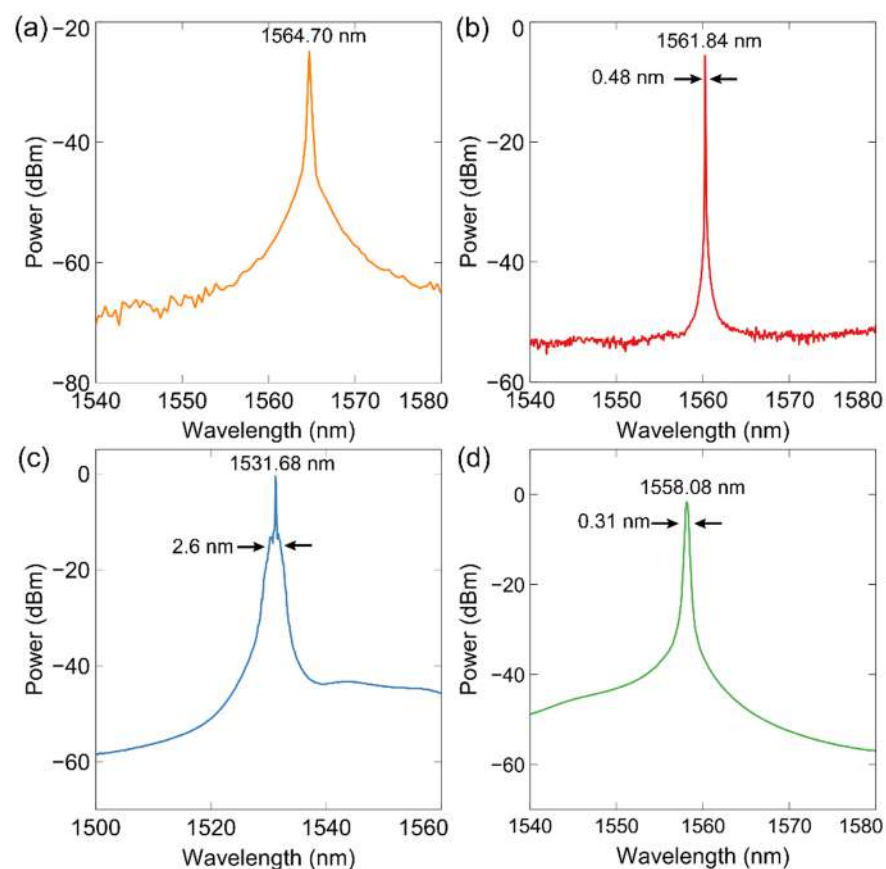


Figure 11. Optical spectrum trace from OSA at maximum pump power for (a) continuous wave, (b) graphene-chitin, (c) MoS₂-chitin, and (d) graphene-MoS₂-chitin.

A broad wavelength spectrum can also be observed when using graphene-MoS₂-chitin based SA with spectral bandwidth of 0.31 nm at 1558.08 nm central wavelength. The observed optical spectrum broadening can be inferred to the self-phase modulation effect in the laser cavity and the nanosecond operation of the EDFL. Meanwhile, MoS₂-chitin based SA produced a broad wavelength of 1531.68 nm with a sharp peak due to parasitic lasing as shown in Figure 11c. Parasitic lasing is an uncontrolled lasing resulting from the internal reflection of light inside laser system, thereby making a highly unsaturated laser gain during pumping period [40]. It can also relate to the uneven dispersion and surface condition of the material [41]. The optical spectrum that exhibits parasitic lasing can reduce the reliability of a high-gain laser [40]. This could probably be one of the hindering factors in generating nanosecond pulsed laser using this specific SA. The low saturable

absorption of MoS₂-chitin SA (as observed in Figure 9b) cannot provide enough gain to produce sufficient optical power and overcome the parasitic lasing [41].

A stable self-started nanosecond pulse was obtained as the input pump power was increased gradually above the threshold of 40.29 mW until 111.52 mW for graphene-MoS₂-chitin and 35.20 mW until 75.91 mW for graphene-chitin. The threshold pump power is relatively high due to the insertion loss of the SA film and the long cavity. As the pump power was further increased, both SA films were observed to maintain their stability without any thermal damage. The stable repetition rate and pulse width were achieved, which denotes that the nanosecond pulse laser operation was able to be maintained until the maximum pump power. Repetition rate of graphene-chitin and graphene-MoS₂-chitin SA was recorded at a similar frequency of 1.89 MHz. This is because the repetition rate is dependent to the length of laser cavity. The oscilloscope trace of the pulse train as illustrated in Figure 12a,b, demonstrated that the time interval between the pulses is about 529 ns, equal to 1.89 MHz which corresponds to the cavity length of 110 m. The shortest pulse width was achieved by graphene-MoS₂-chitin at 156.4 ns and was maintained when adjusting the input pump power from 40.29 mW to 111.52 mW. The recorded nanosecond pulse width is also lower than previous reported SA based on single-walled carbon nanotube (SWCNT) by drop-cast technique at 332 ns [42], zinc oxide-polyvinyl alcohol (PVA) at 400 ns [43], silver nanoparticle-polyvinyl alcohol (AgNP-PVA) at 202 ns [44] and copper nanowires-polydimethylsiloxane (CuNWs-PDMS) film at 173 ns [45] indicating that the developed hybrid graphene SA yielded better performance for nanosecond pulsed laser in EDFL. In comparison with its single component, graphene-chitin has slightly longer pulse width of 186.4 ns, but still shorter than graphene-polyethylene oxide (graphene-PEO) developed by another work [39] that records 400 ns pulse width.

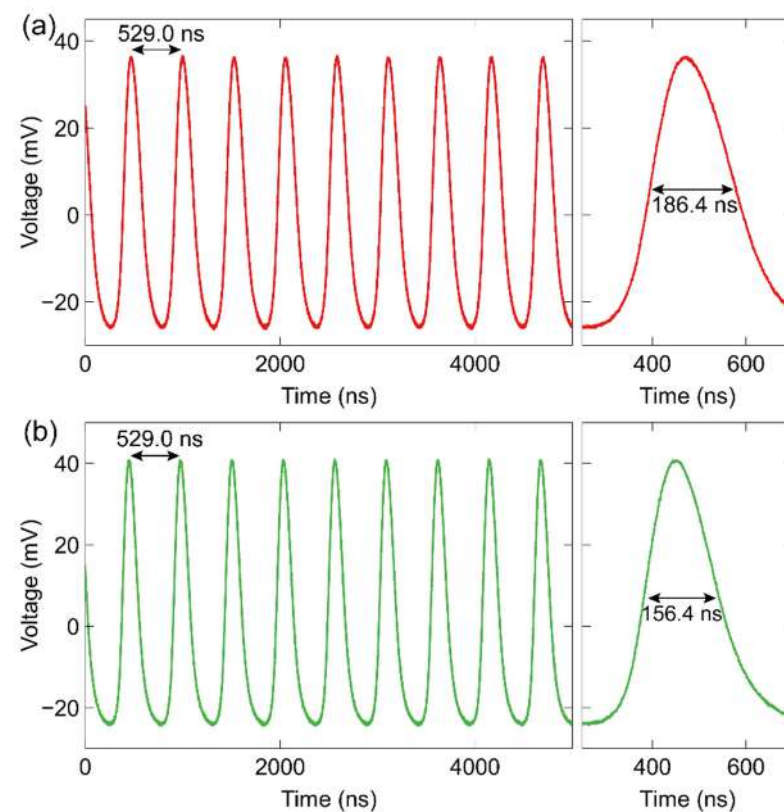


Figure 12. Pulse train recorded by oscilloscope for (a) graphene-chitin and (b) graphene-MoS₂-chitin with respective single pulse profile.

Figure 13a,b show the average output power and pulse energy of the generated laser pulses against pump power. The output power was observed to have a typical increasing

trend with the corresponding pump power. At maximum pump power, peak power and pulse energy recorded by graphene-chitin are 31.71 mW and 5.91 nJ respectively, five times higher than graphene-PEO based SA proposed by Ismail et al., [39] that recorded at about 1.739 mW and 1.79 nJ. Meanwhile, a higher value of peak power and pulse energy was achieved by graphene-MoS₂ than individual graphene-based SA at maximum pump power which was recorded at 56.13 mW and 8.78 nJ respectively. The results demonstrated that the hybrid graphene could generate high-energy pulsed lasers at a high incident laser pump.

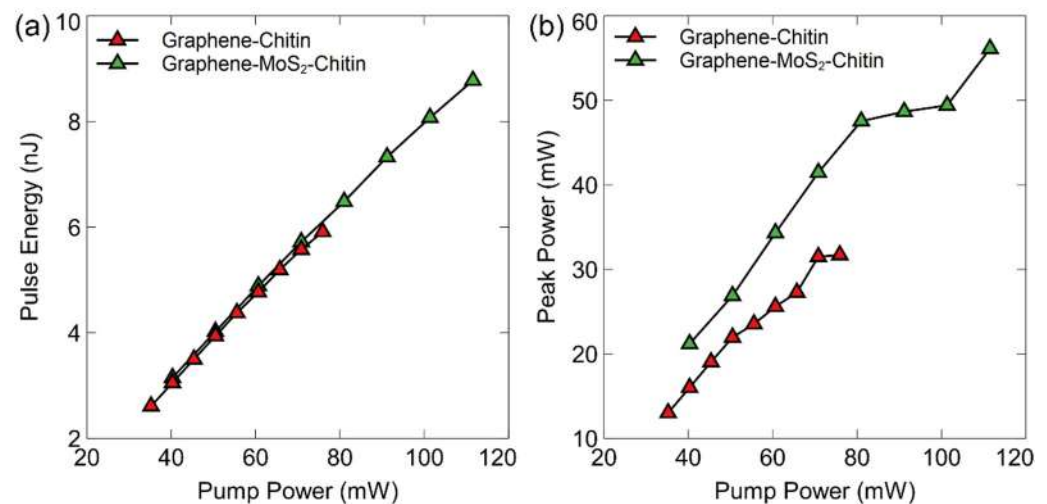


Figure 13. Variation of (a) pulse energy and (b) peak power against pump power of graphene-chitin and graphene-MoS₂-chitin.

Besides, the stability of the pulsed laser was analysed based on the RF spectrum obtained from the RF spectrum analyser as shown in Figure 14a,b. The RF spectrum for both developed SAs show high signal-to-noise ratio (SNR) above ~60 dB which indicate the stability of the pulses with no signal inconsistency. The plotted result also demonstrated the fundamental frequency of 1.89 MHz that matches with the peak-to-peak duration of the oscilloscope pulse period. The SNR value recorded by graphene-chitin and graphene-MoS₂-chitin were 69.06 dB and 67.69 dB respectively, higher than graphene-PEO (57.3 dB) [39], SWCNT (36 dB) [42], ZnO-PVA (64 dB) [43], and CuNWs-PDMS (61 dB) [45]. These results suggest that graphene-MoS₂-chitin hybrid developed through LPE method could be as an effective SA for nanosecond pulse generation and exhibit better SA performance compared to previous reported works [39,42–45]. Finally, the performance of the proposed SA is compared with recent publication of nanosecond EDFL as summarized in Table 1. These results verified the ability of graphene-MoS₂-chitin SA film to generate nanosecond pulsed lasers and their potential applications in optoelectronic devices.

Table 1. Summary for nanosecond pulse laser generation parameters of different materials.

Material for SA	Rep. Rate	Pulse Width (ns)	Central Wavelength (nm)	Pulse Energy (nJ)	Peak Power (mW)	SNR (dB)	Ref.
Graphene-PEO	969.0 kHz	400	1564.0	1.79	1.739	57.3	[39]
SWCNT (drop cast)	909.1 kHz	332	1570.4	0.34	0.31	36.0	[42]
ZnO-PVA	1.0 MHz	400	1558.3	11.6	27.3	64.0	[43]
AgNP-PVA	1.0 MHz	202	1561.5	52.3	2.42	74.3	[44]
CuNW-PDMS	1.86 MHz	173	1563.3	9.15	3.41	61.0	[45]
Graphene-chitin	1.89 MHz	186	1561.8	5.91	31.71	69.1	This work
Graphene-MoS ₂ -chitin	1.89 MHz	156	1558.1	8.78	56.13	67.7	This work

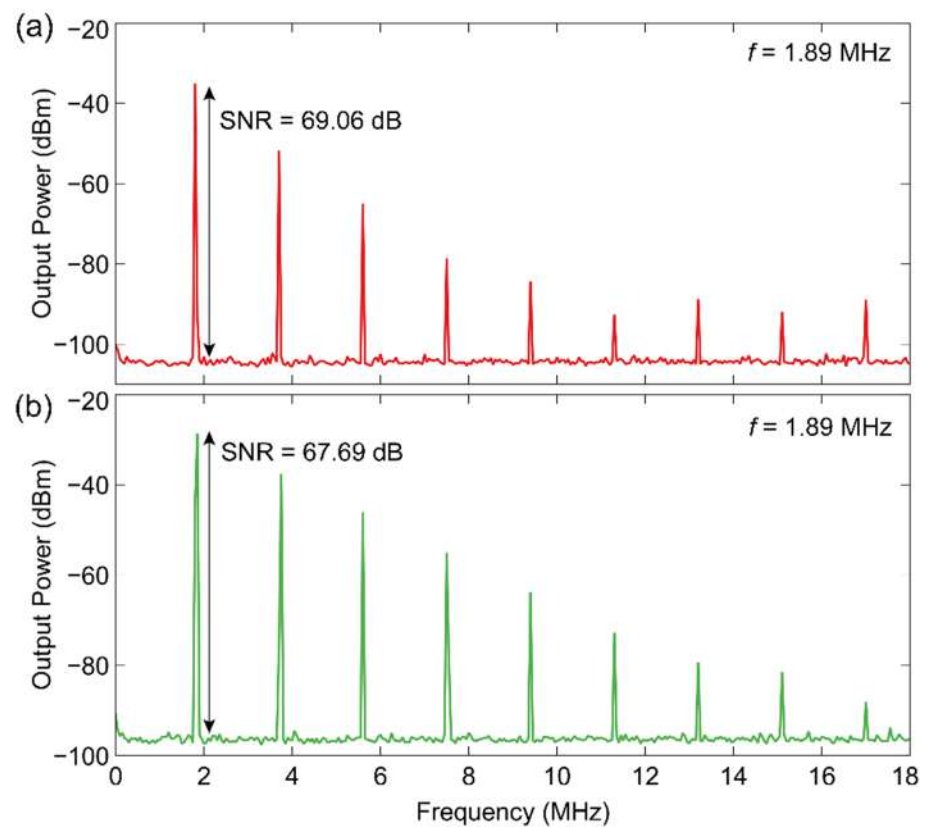


Figure 14. RFSA measurement of (a) graphene-chitin and (b) graphene-MoS₂-chitin SA.

The developed MoS₂-chitin SA yielded a stable Q-switched pulsed laser in the same laser cavity. Figure 15 shows the laser characterisation of MoS₂-chitin SA. At maximum pump power of 136.96 mW, a high repetition rate of 112.3 kHz with very small amplitude jitters and pulse width of 2.61 μs were recorded. The repetition rate was by far the highest recorded value compared to other reported works developed by liquid-phase exfoliation and mechanical exfoliation approach, which is 27.0 kHz [46], 38.43 kHz [47], and 43.47 kHz [48]. A typical Q-switched operation can be observed from the ascending trend of pulse energy and peak power against absorbed pump power. As shown in Figure 15c, the maximum instantaneous peak power of 18.01 mW and pulse energy of 47.02 nJ were obtained at maximum pump power. Next, the RF spectrum was graphed to further verify the stability of the Q-switched lasers. Based on the data illustrated in Figure 15d, it reveals MoS₂-chitin SA’s SNR of up to ~59.27 dB. The obtained value is quite impressive compared to other previous works [46–48]. Table 2 summarizes the Q-switched performance from a few recent studies. Among the list, our developed MoS₂-chitin SA has the highest repetition rate of 112.3 kHz, low pulse width of 2.61 μs, and high SNR value of 59.27 dB.

Table 2. Summarization of Q-switched laser parameters for MoS₂ based materials.

Pulse Width (μs)	Rep. Rate (kHz)	Central Wavelength (nm)	Pulse Energy (nJ)	SNR (dB)	Ref.
5.4	6.5–27.0	1565.0	63.2	54.50	[46]
5.02	14.25–38.43	1551.4	141.3	38.43	[47]
3.3	8.77–43.47	1551.7	160	~50	[48]
2.61	43.35–112.3	1558.1	47.02	59.27	This work

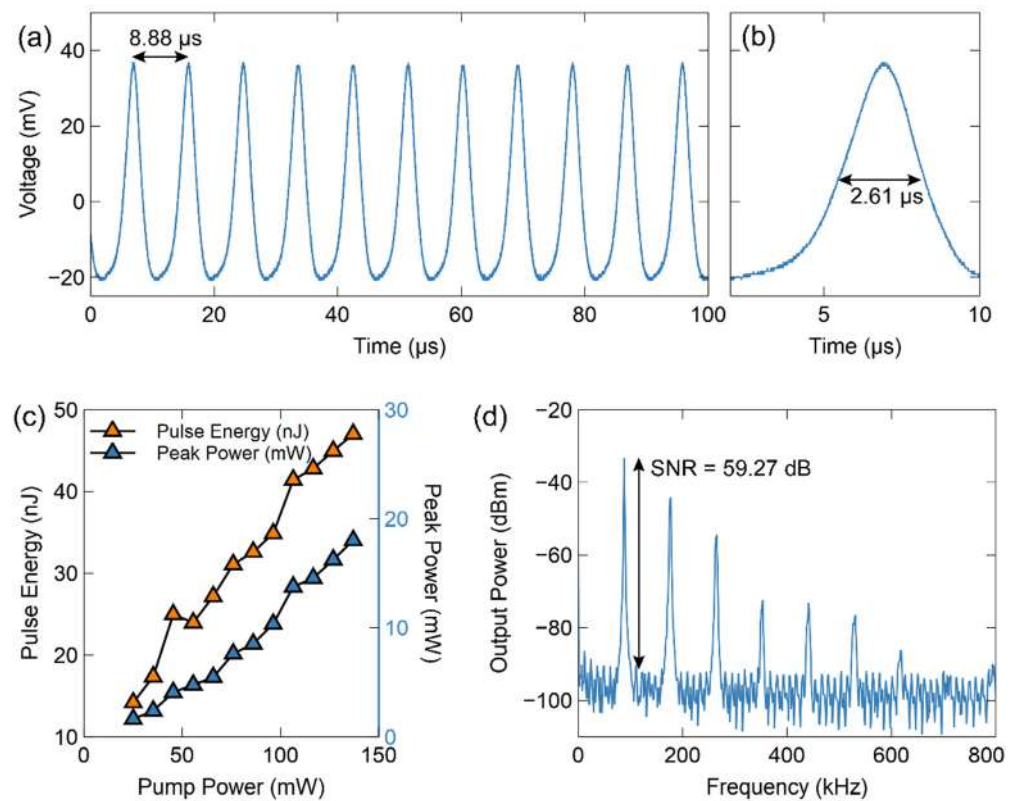


Figure 15. Pump characterisation for MoS₂-chitin SA; (a) Pulse train, (b) single pulse profile with pulse width of 2.61 µs, (c) variation of pulse energy and peak power against pump power, and (d) RFS measurement.

5. Conclusions

Investigation on properties of hybrid graphene-MoS₂ via both theoretical and experimental work is reported in this work. Incorporation of MoS₂ into graphene has led to modification in graphene band gap from 0 eV of graphene and 1.7 eV of MoS₂ to a value of 2 meV with direct transition type. The interlayer coupling between MoS₂ and graphene has been confirmed by Raman spectra. A stable all-fiber erbium-doped fiber laser generating a nanosecond pulse train has been successfully demonstrated using prepared saturable absorber by cost-effective liquid-phase exfoliation method. Using the graphene-MoS₂-chitin, a nanosecond pulse with repetition rate of 1.891 MHz and 154.6 ns pulse width at threshold pump power of 40.29 mW operating at 1558.08 nm was realized. The generated pulsed could find an application in material processing, remote sensing, and other photonic fields.

Author Contributions: Conceptualization, F.A. and S.N.M.H.; methodology, S.N.M.H., W.M.F.W.N., S.W.H., H.H.J.S., H.Y. and S.S.; software, M.F.M.T.; validation, M.F.M.T., F.A. and S.N.M.H.; formal analysis, F.A.; investigation, S.N.M.H.; resources, H.H.J.S., F.A. and H.Y.; writing—original draft preparation, S.N.M.H.; writing—review and editing, S.N.M.H., F.A. and M.Q.L.; visualization, M.F.M.T. and M.Q.L.; supervision, F.A., H.H.J.S. and H.Y.; project administration, F.A.; funding acquisition, M.A.A.R. and F.A. All authors have read and agreed to the published version of the manuscript.

Funding: This research was funded by UTM R&D Fund Tier 2, grant number 17J24 and partially under Professional Development Research University (PDRU), grant number 05E61.

Institutional Review Board Statement: Not applicable.

Informed Consent Statement: Not applicable.

Data Availability Statement: Not applicable.

Acknowledgments: The authors would like to acknowledge Faculty of Applied Science, Universiti Teknologi MARA (UiTM) and Department of Electrical Engineering, Faculty of Engineering, Uni-

versity of Malaya for providing facility and equipment throughout this project. S.N.M.H. would like to thanks Malaysia-Japan International Institute of Technology (MJIT), Universiti Teknologi Malaysia for the scholarship. M.Q.L. also would like to thanks Universiti Teknologi Malaysia for the Postdoctoral Fellowship.

Conflicts of Interest: The authors declare no conflict of interest.

References

- Zhang, B.; Liu, J.; Wang, C.; Yang, K.; Lee, C.; Zhang, H.; He, J. Recent Progress in 2D Material-Based Saturable Absorbers for All Solid-State Pulsed Bulk Lasers. *Laser Photon. Rev.* **2019**, *14*, 1900240. [[CrossRef](#)]
- Bao, Q.; Zhang, H.; Ni, Z.; Wang, Y.; Polavarapu, L.; Shen, Z.; Xu, Q.-H.; Tang, D.; Loh, K.P. Monolayer graphene as a saturable absorber in a mode-locked laser. *Nano Res.* **2010**, *4*, 297–307. [[CrossRef](#)]
- Fu, W.; Wright, L.G.; Sidorenko, P.; Backus, S.; Wise, F.W. Several new directions for ultrafast fiber lasers [Invited]. *Opt. Express* **2018**, *26*, 9432–9463. [[CrossRef](#)] [[PubMed](#)]
- Nawz, T.; Safdar, A.; Hussain, M.; Sung Lee, D.; Siyar, M. Graphene to advanced MoS₂: A review of structure, synthesis, and optoelectronic device application. *Crystals* **2020**, *10*, 902. [[CrossRef](#)]
- Liu, C.-H.; Zheng, J.; Colburn, S.; Fryett, T.K.; Chen, Y.; Xu, X.; Majumdar, A. Ultrathin van der Waals Metalenses. *Nano Lett.* **2018**, *18*, 6961–6966. [[CrossRef](#)]
- Giovannetti, G.; Khomyakov, P.A.; Brocks, G.; Kelly, P.J.; Van Den Brink, J. Substrate-induced band gap in graphene on hexagonal boron nitride: Ab initio density functional calculations. *Phys. Rev. B* **2007**, *76*, 073103. [[CrossRef](#)]
- Sun, J.; Lin, N.; Tang, C.; Wang, H.; Ren, H.; Zhao, X. First principles studies on electronic and transport properties of edge contact graphene-MoS₂ heterostructure. *Comput. Mater. Sci.* **2017**, *133*, 137–144. [[CrossRef](#)]
- Xia, C.; Xiong, W.; Xiao, W.; Du, J.; Fang, L.; Li, J.; Jia, Y. Enhanced carrier concentration and electronic transport by inserting graphene into van der Waals heterostructures of transition-metal dichalcogenides. *Phys. Rev. Appl.* **2018**, *10*, 24–28. [[CrossRef](#)]
- Hu, W.; Yang, J. First-principles study of two-dimensional van der Waals heterojunctions. *Comput. Mater. Sci.* **2016**, *112*, 518–526. [[CrossRef](#)]
- Sun, X.; Zhang, B.; Li, Y.; Luo, X.; Li, G.; Chen, Y.; Zhang, C.; He, J. Tunable ultrafast nonlinear optical properties of graphene/MoS₂ van der Waals heterostructures and their application in solid-state bulk lasers. *ACS Nano* **2018**, *12*, 11376–11385. [[CrossRef](#)]
- Zhao, G.; Hou, J.; Wu, Y.; He, J.; Hao, X. Preparation of 2D MoS₂/graphene heterostructure through a monolayer intercalation method and its application as an optical modulator in pulsed laser generation. *Adv. Opt. Mater.* **2015**, *3*, 937–942. [[CrossRef](#)]
- Du, W.; Li, H.; Lan, C.; Li, C.; Li, J.; Wang, Z.; Liu, Y. Graphene/WS₂ heterostructure saturable absorbers for ultrashort pulse generation in L-band passively mode-locked fiber lasers. *Opt. Express* **2020**, *28*, 11514–11523. [[CrossRef](#)]
- Li, Z.; Cheng, C.; Dong, N.; Romero, C.; Lu, Q.; Wang, J.; de Aldana, J.R.V.; Tan, Y.; Chen, F. Q-switching of waveguide lasers based on graphene/WS₂ van der Waals heterostructure. *Photon. Res.* **2017**, *5*, 406–410. [[CrossRef](#)]
- Bonaccorso, F.; Sun, Z.; Hasan, T.; Ferrari, A.C. Graphene photonics and optoelectronics. *Nat. Photon.* **2010**, *4*, 611–622. [[CrossRef](#)]
- Adetayo, A.; Runsewe, D. Synthesis and Fabrication of Graphene and Graphene Oxide: A Review. *Open J. Compos. Mater.* **2019**, *9*, 207–229. [[CrossRef](#)]
- Demir, M.M.; Wegner, G. Challenges in the Preparation of Optical Polymer Composites with Nanosized Pigment Particles: A Review on Recent Efforts. *Macromol. Mater. Eng.* **2012**, *297*, 838–863. [[CrossRef](#)]
- Jiang, Y.; Miao, L.; Jiang, G.; Chen, Y.; Qi, X.; Jiang, X.F.; Zhang, H.; Wen, S. Broadband and enhanced nonlinear optical response of MoS₂/graphene nanocomposites for ultrafast photonics applications. *Sci. Rep.* **2015**, *5*, 16372. [[CrossRef](#)]
- Feng, Y.; Dong, N.; Wang, G.; Li, Y.; Zhang, S.; Wang, K.; Zhang, L.; Blau, W.J.; Wang, J. Saturable absorption behavior of free-standing graphene polymer composite films over broad wavelength and time ranges. *Opt. Express* **2015**, *23*, 559–569. [[CrossRef](#)] [[PubMed](#)]
- Kumar, A.K.S.; Zhang, Y.; Li, D.; Compton, R.G. A mini-review: How reliable is the drop casting technique? *Electrochem. Commun.* **2020**, *121*, 106867. [[CrossRef](#)]
- Zuikafly, S.N.F.; Nawawi, W.W.; Ngee, L.H.; Yahaya, H.; Yahya, W.J.; Ahmad, F. November. Graphene in chitin based passive Q-switcher. *J. Phys. Conf. Ser.* **2019**, *1371*, 012011. [[CrossRef](#)]
- Yang, C.-H.; Chang, S.-T. First-Principles Study of the Optical Properties of TMDC/Graphene Heterostructures. *Photonics* **2022**, *9*, 387. [[CrossRef](#)]
- Phuc, H.V.; Hieu, N.N.; Hoi, B.D.; Phuong, L.T.; Nguyen, C.V. First principle study on the electronic properties and Schottky contact of graphene adsorbed on MoS₂ monolayer under applied out-plane strain. *Surf. Sci.* **2018**, *668*, 23–28. [[CrossRef](#)]
- Singh, S.; Espejo, C.; Romero, A.H. Structural, electronic, vibrational, and elastic properties of graphene/MoS₂ bilayer heterostructures. *Phys. Rev. B* **2018**, *98*, 155–309. [[CrossRef](#)]
- Qiu, B.; Zhao, X.; Hu, G.; Yue, W.; Ren, J.; Yuan, X. Optical Properties of Graphene/MoS₂ Heterostructure: First Principles Calculations. *Nanomaterials* **2018**, *8*, 962. [[CrossRef](#)] [[PubMed](#)]
- Hieu, N.N.; Ilyasov, V.V.; Vu, T.V.; Poklonski, N.A.; Phuc, H.V.; Phuong, L.T.; Hoi, B.D.; Nguyen, C.V. First principles study of optical properties of molybdenum disulfide: From bulk to monolayer. *Superlattices Microstruct.* **2018**, *115*, 10–18. [[CrossRef](#)]

26. Pierucci, D.; Henck, H.; Avila, J.; Balan, A.; Naylor, C.H.; Patriarche, G.; Dappe, Y.J.; Silly, M.G.; Sirotti, F.; Johnson, A.T.C.; et al. Band Alignment and Minigaps in Monolayer MoS₂-Graphene van der Waals Heterostructures. *Nano Lett.* **2016**, *16*, 4054–4061. [CrossRef]
27. Rani, P.; Dubey, G.S.; Jindal, V. DFT study of optical properties of pure and doped graphene. *Phys. E Low-Dimens. Syst. Nanostruct.* **2014**, *62*, 28–35. [CrossRef]
28. Tuz Johra, F.; Lee, J.-W.; Jung, W.-G. Facile and safe graphene preparation on solution based platform. *J. Ind. Eng. Chem.* **2014**, *20*, 2883–2887. [CrossRef]
29. Zeranska-Chudek, K.; Łapińska, A.; Wroblewska, A.; Judek, J.; Dużyńska, A.; Pawłowski, M.; Witowski, A.; Zdrojek, M. Study of the absorption coefficient of graphene-polymer composites. *Sci. Rep.* **2018**, *8*, 9132. [CrossRef] [PubMed]
30. Ponraj, J.S.; Xu, Z.; Dhanabalan, S.C.; Mu, H.; Wang, Y.; Yuan, J.; Li, P.; Thakur, S.; Ashrafi, M.; McCoubrey, K.; et al. Photonics and optoelectronics of two-dimensional materials beyond graphene. *Nanotechnology* **2016**, *27*, 462001. [CrossRef] [PubMed]
31. Black Magic 3D conductive graphene composites 1.75 mm. Available online: <https://3dcompare.com/materials/product/black-magic-3d-conductive-graphene-composite-1-75-mm> (accessed on 12 May 2022).
32. Nawawi, W.M.F.W.; Lee, K.-Y.; Kontturi, E.; Murphy, R.J.; Bismarck, A. Chitin Nanopaper from Mushroom Extract: Natural Composite of Nanofibers and Glucan from a Single Biobased Source. *ACS Sustain. Chem. Eng.* **2019**, *7*, 6492–6496. [CrossRef]
33. Li, Z.; Young, R.J.; Backes, C.; Zhao, W.; Zhang, X.; Zhukov, A.; Tillotson, E.; Conlan, A.P.; Ding, F.; Haigh, S.J.; et al. Mechanisms of Liquid-Phase Exfoliation for the Production of Graphene. *ACS Nano* **2020**, *14*, 10976–10985. [CrossRef]
34. Lokman, M.Q.; Rusdi, M.F.M.; Rosol, A.H.A.; Ahmad, F.; Shafie, S.; Yahaya, H.; Rosnan, R.M.; Rahman, M.A.A.; Harun, S.W. Synthesis of silver nanoparticles using chemical reduction techniques for Q-switcher at 1.5 μm region. *Optik* **2021**, *244*, 167621. [CrossRef]
35. Wall, M. The Raman spectroscopy of graphene and the determination of layer thickness. *Thermo Sci.* **2011**, *5*, 1–5.
36. Zheng, X.; Zhang, H.; Yang, Q.; Xiong, C.; Li, W.; Yan, Y.; Gurney, R.S.; Wang, T. Solution-processed Graphene-MoS₂ heterostructure for efficient hole extraction in organic solar cells. *Carbon* **2018**, *142*, 156–163. [CrossRef]
37. Makuła, P.; Pacia, M.; Macyk, W. How to correctly determine the band gap energy of modified semiconductor photo-catalysts based on UV-Vis spectra. *J. Phys. Chem. Lett.* **2018**, *9*, 6814–6817. [CrossRef]
38. Lin, J.H.; Huang, G.H.; Ou, C.H.; Che, K.C.; Liu, W.R.; Tasy, S.Y.; Chen, Y.H. Q-Switched pulse and mode-locked pulse generation from a Yb³⁺-Doped fiber laser based on Bi₂Se₃. *IEEE Photonics J.* **2018**, *10*, 1–10. [CrossRef]
39. Ismail, M.K.; Markom, A.M.; Rusdi, M.F.M.; Jafry, A.A.A.; Samsamun, F.S.M.; Rosol, A.H.A.; Zakaria, Z. Nanosecond Generation in An Erbium-Doped Fiber Laser Using Graphene Material. *J. Fotonik* **2020**, *1*, 13–17.
40. Storm, M.E. Controlled retroreflection: A technique for understanding and eliminating parasitic lasing. *J. Opt. Soc. Am. B* **1992**, *9*, 1299–1304. [CrossRef]
41. Mashkin, A.; Fomin, V.; Shcherbina, F.; Dronov, A.; Abramov, A.; Mironov, V.; Scherbakov, E. Fiber Laser System with Mechanism for Inducing Parasitic Lights Losses. U.S. Patent 17/119,361, 11 December 2020.
42. Ismail, M.A.; Harun, S.W.; Zulkepely, N.R.; Nor, R.; Ahmad, F.; Ahmad, H. Nanosecond soliton pulse generation by mode-locked erbium-doped fiber laser using single-walled carbon-nanotube-based saturable absorber. *Appl. Opt.* **2012**, *51*, 8621–8624. [CrossRef] [PubMed]
43. Alani, I.A.M.; Ahmad, B.A.; Ahmed, M.H.M.; Latiff, A.A.; Al-Masoodi, A.H.H.; Lokman, M.Q.; Harun, S.W. Nanosecond mode-locked erbium doped fiber laser based on zinc oxide thin film saturable absorber. *Indian J. Phys.* **2018**, *93*, 93–99. [CrossRef]
44. Rosdin, R.Z.R.R.; Ahmad, M.T.; Muhammad, A.R.; Jusoh, Z.; Arof, H.; Harun, S.W. Nanosecond Pulse Generation with Silver Nanoparticle Saturable Absorber. *Chin. Phys. Lett.* **2019**, *36*, 054202. [CrossRef]
45. Ismail, E.; Ahmad, F.; Shafie, S.; Yahaya, H.; Latif, A.; Muhammad, F. Copper nanowires based mode-locker for soliton nanosecond pulse generation in erbium-doped fiber laser. *Results Phys.* **2020**, *18*, 103228. [CrossRef]
46. Luo, Z.; Huang, Y.; Zhong, M.; Li, Y.; Wu, J.; Xu, B.; Xu, H.; Cai, Z.; Peng, J.; Weng, J. 1-, 1.5-, and 2-μm fiber lasers Q-switched by a broadband few-layer MoS₂ saturable absorber. *J. Lightwave Technol.* **2014**, *32*, 4077–4084. [CrossRef]
47. Ahmed, M.H.M.; Al-Masoodi, A.H.H.; Latiff, A.A.; Arof, H.; Harun, S.W. Mechanically exfoliated 2D nanomaterials as saturable absorber for Q-switched erbium doped fiber laser. *Indian J. Phys.* **2017**, *91*, 1259–1264. [CrossRef]
48. Huang, Y.; Luo, Z.; Li, Y.; Zhong, M.; Xu, B.; Che, K.; Xu, H.; Cai, Z.; Peng, J.; Weng, J. Widely-tunable, passively Q-switched erbium-doped fiber laser with few-layer MoS₂ saturable absorber. *Opt. Express* **2014**, *22*, 25258–25266. [CrossRef] [PubMed]